TECHNICAL NOTE

Nondiffracting interference patterns generated with programmable spatial light modulators

Jeffrey A. Davis, E. Carcole, and Don M. Cottrell

Nondiffracting beams are of interest for optical metrology applications because the size and shape of the beams do not change as the beams propagate. We have created a generating pattern consisting of a linear combination of two nondiffracting patterns. This pattern forms a nondiffracting interference pattern that appears as a circular array of nondiffracting spots. More complicated multiplexed arrays are also constructed that simultaneously yield two different nondiffracting patterns. We generate these Bessel function arrays with a programmable spatial light modulator. Such arrays would be useful for angular alignment and for optical interconnection applications.

Key words: Nondiffracting beams, Bessel function beams, spatial light modulators, diffractive optical elements.

Nondiffracting zero-order Bessel function beams[1,2] are of interest for such applications as optical alignment, surveying, industrial inspection, and optical interconnections. Higher-order[3] Bessel function beams have also been generated. These higher-order nondiffracting Bessel function beams have a zero axial irradiance, and the size of the dark spot for the first-order Bessel function beam is smaller than the size of the corresponding bright spot from the zero-order Bessel function beam. In other recent research[4] multiplexed patterns were formed that created separated arrays of these nondiffracting beams.

In this research, we create a generating pattern consisting of a linear combination of two spatially overlapping nondiffracting patterns. This pattern forms a nondiffracting interference pattern that appears as a circular array of nondiffracting spots. The diameter of the array and the number of spots within the array can be varied by changing the generating pattern. In addition we combine a nondiffracting interference pattern with a first-order Bessel function beam by multiplexing the different generating patterns. When these patterns are created with a programmable spatial light modulator (SLM), all of these characteristics can be altered.

Higher-order nondiffracting Bessel function beams can be created with a hologram[2,3] with an angular phase shift such as

$$T_n(r, \theta) = \exp(in\theta)\exp(-i2\pi r/r_0), \tag{1}$$

where θ and r are coordinates in the hologram plane, r_0 is an adjustable scale factor, and n is an integer.

The electric field representing an nth-order Bessel function $J_n(\rho)$ that is formed at a distance z from the plane of the hologram is given[2,3] by

$$E(\rho, \phi) \approx J_n\left(\frac{2\pi\rho}{r_0}\right)\exp(in\phi). \tag{2}$$

Here ρ and ϕ are coordinates in the observation plane. The beam width for the zero-order Bessel function beam is given (in the small angle approximation) by $W_0 = 0.766r_0$. The widths of the higher-order beams increase approximately linearly with n as $W_n \approx 0.766nr_0$. The amplitude of the electric field[2,3] increases as $\sqrt{z}$ (with some oscillations) to a maximum value at a distance of roughly $L = Rr_0/\lambda$ and then sharply decreases. The widths of all the Bessel function beams remain constant over this distance of approximately L.

In this research we construct a new hologram containing a linear combination from Eq. (1) as

$$T_n(r, \theta) = \{\exp[i(n\theta + \alpha)] + \exp[-i(n\theta - \alpha)]\} \times \exp(-i2\pi r/r_0), \tag{3}$$

The authors are with the Department of Physics, San Diego State University, San Diego, California 92182. E. Carcole's permanent address is the Departament de Fisica, Universitat Autonoma de Barcelona, Bellaterra 08193, Spain.

Received 21 April 1995; revised manuscript received 2 October 1995.

0003-6935/96/040599-04$06.00/0

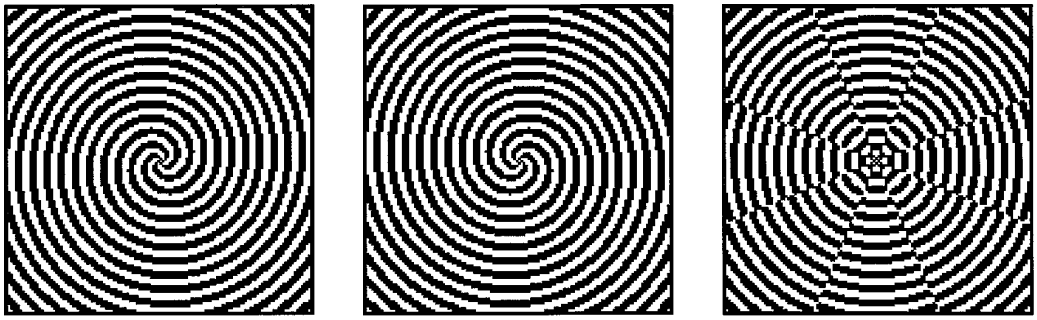

(a) (b) (c)

Fig. 1. Binary patterns written onto the SLM that form (a) the J_4 Bessel function beam where $q = 6$, (b) the J_{-4} Bessel function beam where $q = 6$, (c) linear combination of the J_4 and the J_{-4} Bessel function beams where $q = 6$.

where α is a constant. Following the discussion above, this pattern produces an electric field given by

$$E(\rho, \phi) \approx J_n\left(\frac{2\pi\rho}{r_0}\right)[\exp[i(n\phi + \alpha)] + \exp[-i(n\phi - \alpha)]]. \tag{4}$$

Consequently an intensity pattern is observed that is given by

$$I(\rho, \phi) \approx J_n^2\left(\frac{2\pi\rho}{r_0}\right)\cos^2(n\theta + \alpha). \tag{5}$$

The $J_n^2(2\pi\rho/r_0)$ term appears as a circular intensity pattern with a radius associated with the nth-order Bessel function. However, the intensity is azimuthally modulated, resulting in a series of $2n$ spots arranged on a circle. The angular alignment of the circular array of spots can be rotated by varying the angle α.

The patterns of Eqs. (1) and (3) can be encoded[5,6] onto a SLM by writing $r^2 = (i^2 + j^2)(\Delta^2)$, where i and j are integers identifying each pixel and Δ is the pixel spacing. In this case, $r_0 = q\Delta$, where q is an adjustable parameter, N is the number of pixels in the SLM, and the size of the hologram can be written as $R = N\Delta/2$.

Figure 1(a) shows the hologram from Eq. (1) that encodes the J_4 Bessel function for parameters $n = 4$, $q = 6$. The pattern is characterized by the spiral arms multiplying the radial grating. Figure 1(b) shows the pattern for parameters $n = -4$, $q = 6$, and the spiral arms rotate in the opposite sense. Figure 1(c) shows the pattern from Eq. (3) for the linear combination of these patterns, where $\alpha = 0$.

These masks were written onto a magneto-optic spatial light modulator[7] (MOSLM), manufactured by Semetex Corporation, operating in the binary phase-only mode.[8] The MOSLM has a pixel size of $\Delta = 75$ μm and $N = 128$. In all cases, binary phase-only versions of these patterns were written onto the SLM. The binarization process[6] causes higher-order versions of the Bessel function beams to be generated that have smaller diameters and shorter propagation distances. The effects of these higher-order beams can be avoided by working at sufficiently large distances where these higher-order beams are attenuated.

The MOSLM was illuminated with collimated light from a He–Ne laser, and the output beam was recorded with a CCD camera with a pixel size of 12 μm connected to the Macintosh computer through a ComputerEyes interface system. It is critical that the aberrations from the SLM be corrected[9] to generate these output beams. Otherwise the electric-field profile is strongly distorted.

Figure 2(a) shows the intensity for the pattern associated with either Fig. 1(a) or 1(b) measured at a distance of 1.55 m from the MOSLM with a CCD camera. The image sizes are approximately 1.5

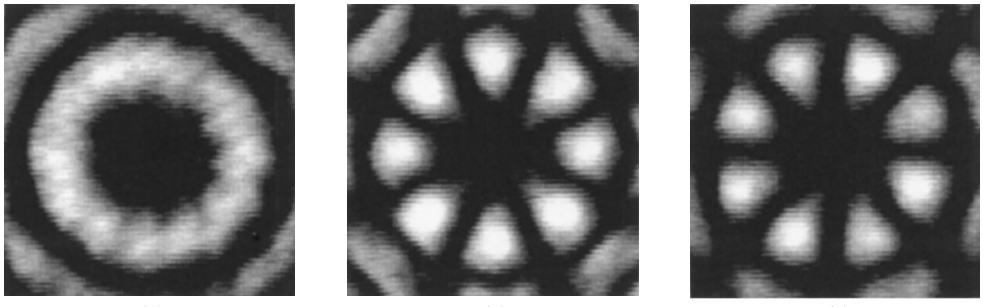

(a) (b) (c)

Fig. 2. Output intensities measured at a distance of 1.55 m from the MOSLM: (a) The intensity for the J_4 Bessel function beam where $q = 6$ is generated from Fig. 1(a) or 1(b). (b) The circular spot array for $n = 4$, $q = 6$ generated from Fig. 1(c). The output is an array of $2n = 8$ spots. (c) The circular spot array for $n = 4$, $q = 6$ rotated by an angle of $\alpha = 22.5$ deg. The output array is rotated accordingly.

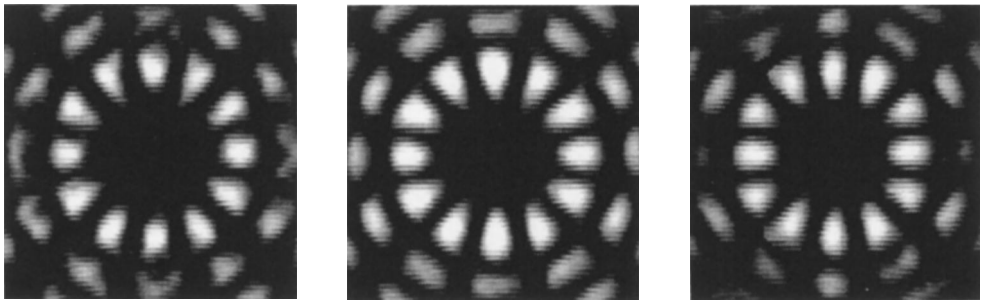

(a) (b) (c)

Fig. 3. Circular spot array for $n = 6, q = 4$. The output is an array of $2n = 12$ spots. Intensities are measured at distances of (a) 0.9 m, (b) 1.55 m, (c) 2.20 m.

mm × 1.5 mm. These two holograms produce indistinguishable output intensities. Figure 2(b) shows the intensity produced by the composite hologram from Fig. 1(c). The output now consists of a circular array of $2n = 8$ spots. When an angle, $\alpha = 22.5$ deg, is added onto the hologram, the orientation of the spots is rotated as shown in Fig. 2(c). As expected for the intensity of Eq. (4) the dark spaces are narrower than the bright spaces and this might be more useful for angular alignment purposes.

As discussed above the number of spots depends on the number n and the diameter of the array of spots can be changed by changing products n and q. Figure 3(a) shows experimental results for the case in which $n = 6$ and $q = 4$ measured at a distance of 0.9 m from the MOSLM. Again the image sizes are approximately 1.5 mm × 1.5 mm. The radius of the circular array of spots is given by $W_n = 0.766nq\Delta$ and is proportional to the product of nq. Therefore the radius of the circular array in Fig. 3(a) is approximately equal to that of Fig. 2(b) because the product of nq remains the same. However, the number of spots has been increased to $2n = 12$. The array of spots is also nondiffracting. Figures 3(b) and 3(c) show the pattern measured at distances of 1.55 and 2.20 m from the MOSLM.

More complicated arrays can be generated by multiplexing different patterns onto a single hologram. For example, the higher-order spot arrays can be combined with the first-order Bessel function beam. This would simultaneously allow angular alignment (with the higher-order Bessel function spot array) and precise location of the circular axis (given by the dark spot of the first-order Bessel function beam). Care must be taken to ensure that there is negligible interference between the two beams. This is done by choosing a large value for n and two different values for coefficient r_0. Accordingly a new pattern is generated as

$$T_1(r, r_{0A}, \theta) + T_n(r, r_{0B}, \theta) = \chi \exp(i\theta)\exp(-i2\pi r/r_{0A}) + \eta[\exp(in\theta) + \exp(-in\theta)]\exp(-i2\pi r/r_{0B}), \quad (6)$$

where r_{0A} and r_{0B} represent the parameters defining the sizes of the two patterns and χ and η represent scaling parameters that allow the relative sizes of the two beams to be varied.

The output from this pattern (assuming that the interference between the two electric fields can be neglected) is given by

$$I(\rho, \phi) \approx \chi^2 J_1^2\left(\frac{2\pi\rho}{r_{0A}}\right) + \eta^2 J_n^2\left(\frac{2\pi\rho}{r_{0B}}\right)\cos^2(n\phi). \quad (7)$$

Figure 4 shows experimental results. The mask is shown in Fig. 4(a) where $r_{0A} = 4\Delta$, $r_{0B} = 6\Delta$, $n = 16$, $\chi = 0.3$, and $\eta = 1$. The resulting intensity pattern in Fig. 4(b) was measured at a distance of 1.55 m and shows the first-order nondiffracting beam at the center and the 32-spot circular array surrounding it. The area of the circular spot array is much larger than in Fig. 3 because of the large value for nr_{0B}. Therefore the figure shows a larger area equal to 3.6 mm × 3.6 mm. As with previous patterns this intensity pattern is nondiffracting.

In conclusion, we have generated a nondiffracting interference pattern that appears as a circular array of nondiffracting spots. The number of spots, the overall diameter of the circular array, and the angular alignment of the spots can be programmed with programmable SLM's. We also show a multiplexed array that simultaneously creates the nondiffracting interference pattern as well as a centered beam. We expect that these results might be useful for machine vision and surveying applications as well as for optical interconnection networks.

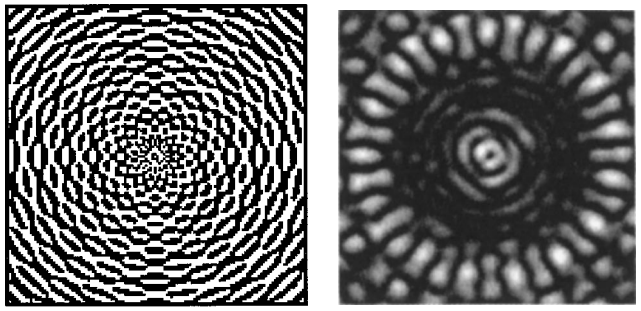

(a) (b)

Fig. 4. (a) Mask that simultaneously generates the J_1 beam (for $q = 4$) and the circular spot array for $n = 16, q = 6$. (b) The output intensity pattern with the pattern shown in (a).

One of us (E. Carcole) acknowledges grant BE94/1-58 Annex-1 from Generalitat de Catalunya, Catalunya, Spain.

References

1. J. Durnin, J. J. Miceli, Jr., and J. H. Eberly, "Diffraction-free beams," Phys. Rev. Lett. **58,** 1499–1501 (1987).
2. J. Turunen, A. Vasara, and A. T. Friberg, "Holographic generation of diffraction-free beams," Appl. Opt. **27,** 3959–3962 (1988).
3. A. Vasara, J. Turunen, and A. T. Friberg, "Realization of general nondiffracting beams with computer-generated holograms," J. Opt. Soc. Am. A **6,** 1748–1754 (1989).
4. R. Piestun and J. Shamir, "Control of wave-front propagation with diffractive elements," Opt. Lett. **19,** 771–773 (1994).
5. J. A. Davis, J. Guertin, and D. M. Cottrell, "Diffraction-free beams generated with programmable spatial light modulators," Appl. Opt. **32,** 6368–6370 (1993).
6. J. A. Davis, E. Carcole, and D. M. Cottrell, "Intensity and phase measurements of nondiffracting beams generated with a magneto-optic spatial light modulator," Appl. Opt. **35,** 593–598 (1996).
7. W. E. Ross, D. Psaltis, and R. H. Anderson, "Two-dimensional magneto-optic spatial light modulator for signal processing," Opt. Eng. **22,** 485–490 (1983).
8. D. Psaltis, E. G. Paek, and S. S. Venkatesh, "Optical image correlation with a binary spatial light modulator," Opt. Eng. **23,** 698–704 (1984).
9. E. Carcole, J. A. Davis, and D. M. Cottrell, "Astigmatic phase correction for the magneto-optic spatial light modulator," Appl. Opt. **34,** 5118–5120 (1995).